KLF2 regulates neural differentiation of dental pulp-derived stem cells by modulating autophagy and mitophagy

Hiranmoy Das (hiranmoy.das@ttuhsc.edu)
Texas Tech University Health Sciences Center https://orcid.org/0000-0002-3343-0096
Prateeksha Prateeksha
TTUHSC
Prathyusha Naidu
Texas Tech University Health Sciences Center
Manjusri Das
Texas Tech University Health Sciences Center
Derek Barthels
Texas Tech University Health Sciences Center

Article

Keywords: KLF2, neural differentiation, DPSC, autophagy, mitophagy

Posted Date: October 20th, 2022

DOI: https://doi.org/10.21203/rs.3.rs-2129477/v1

Abstract

Transplantation of stem cells for treating neurodegenerative disorders is a promising future therapeutic approach. However, the molecular mechanism underlying the neuronal differentiation of mesenchymal stem cells remains inadequately explored. Therefore, the current study aims to define the regulatory role of KLF2 (Kruppel-like factor 2) during the neural differentiation (ND) of dental pulp-derived stem cells (DPSC). Herein, we showed that the expression level of KLF2, autophagy and mitophagy-associated markers were significantly elevated during ND of DPSC. We next validated our results using the chemical-mediated loss- and gain-of-function approaches. We found that the KLF2 inhibitor, GGPP (geranylgeranyl pyrophosphate) significantly reduces the ND of DPSC. Inversely, KLF2 overexpression was accomplished by using the KLF2 inducer, GGTI-298 (geranylgeranyl transferase inhibitor-298) which accelerated the molecular phenomenon of DPSC's commitment towards ND, indicating the crucial function of KLF2 in neurogenesis. Moreover, we found that the KLF2 positively regulated autophagy, mitophagy, and the Wnt5a signaling pathway during neurogenesis. Furthermore, we measured the oxygen consumption rate (OCR), and the extracellular acidification rate (ECAR) during ND in the presence of a KLF2 inducer or KLF2 inhibitor using the Xeflux analyzer. We found that most of the ECAR and OCR parameters were significantly increased during ND and inhibition of KLF2 marginally reversed them towards DPSC's cellular bioenergetics. However, KLF2 overexpression shifted the cellular energy metabolism towards quiescent. Cumulatively, our findings provide the first evidence that the KLF2 critically regulates the neurogenesis of DPSC by inducing autophagy and mitophagy.

Introduction

Neurodegenerative diseases occur due to the progressive loss of structure, function, or number of neurons, sub-sequentially leading to loss of cognition and sensation (1). Stem cell-based therapy has been emerging as a promising hope over other treatment options for all neurodegenerative diseases because stem cells' commitment and differentiation efficacy towards neuronal lineages makes them suitable for repairing the neuronal tissue by transplanting the differentiated neural-like cells (2, 3). Additionally, stem cells possess immunomodulatory and neuroprotective properties, which aid in ameliorating continuous neuron degradation (4, 5). Over the past few decades, extensive preclinical research has been done to prove the therapeutic efficacy of different stem cells, including mesenchymal stem cells, embryonic stem cells, and induced pluripotent stem cells for neurodegenerative disorders (6, 7).

Human dental pulp stem cells (DPSC) exfoliate from the third molar teeth of humans and are of particular interest for clinical purposes because of their relative ease in accessibility, self-renewal, and multi-potency in bone, dental, and neural tissue regeneration (8). DPSC express mesenchymal markers, including CD73, CD90, CD105, CD146, and STRO-1 (9). Moreover, DPSC showed comparatively higher innate potential for neuronal differentiation due to their embryonic neural crest origin during development (10, 11). Additionally, these cells expressed basal levels of neuronal markers such as PAX6, GBX2, and Nestin (12). Therefore, DPSC potentially cured neuronal loss in animal models of several damaged

central nervous systems (CNS), such as spinal cord injury, stroke, Parkinson's disease, Alzheimer's disease, and retinal degeneration (13–15). Recent studies suggested that transplantation of pre-differentiated mesenchymal stem cells (MSCs) exhibits a better therapeutic effect in the *in vivo* model system (16, 17). Several studies established the *in vitro* model system to induce the neuronal differentiation of DPSC. (18–20). However, a better understanding of the molecular signatures that occurred during neuronal differentiation of DPSC is imperative to enhance our in-depth knowledge of neurogenesis and develop more rational regenerative therapy for treating neurodegenerative diseases effectively.

Autophagy is a highly conserved catabolic pathway involved in self-renewal, differentiation of cells, and embryonic development, and acts as an intracellular caretaker by providing the nutrients for cellular functions and selectively eliminating the residual cytosolic wastes, damaged mitochondria, and toxic protein aggregates (21). The formation of autophagosomes, double membrane-bound vesicles, initiates autophagy, the fusion of autophagosomes with lysosomes forms autolysosomal vesicles, which degrades autophagic cargos and the subsequent recycling of macromolecules precursors. Selective elimination of damaged mitochondria through autophagy is known as mitophagy (22, 23). Accumulating data suggest that autophagy and mitophagy play a critical role during the neural differentiation (ND) of stem cells to meet the desire for a high amount of energy and nutrition. Autophagy and mitophagy also regulate several other signaling pathways involved in adequate ND (24–26). Understanding the transcriptional regulators of such pathways will open new avenues in regenerative medicine.

Krüppel-like transcription factors (KLFs), a novel family of transcription factors, are implicated in regulating proinflammatory activation of myeloid cells (27), cell proliferation, and differentiation (28). KLF2, a principal member of the KLFs family, contains highly conserved Cys-2/His-2 zinc-finger domains that bind to the GC-rich region and CACCC-elements of DNA sequences in the promoter of their downstream targets, acting as transcriptional activators or repressors (29). Previous studies reported that KLF2 underpins a broad range of biological functions such as neovascularization, endothelial and bone cell proliferation and function (30, 31), maintenance of B cell homeostasis and plasma cell homing (32), mediation of the granulocyte inflammatory response (33), immune cell function (29), and promotion of inflammatory T cells. Previously, our lab demonstrated that KLF2 plays a critical role in maintaining bone homeostasis through the modulation of autophagy and mitochondrial functions. (31, 34) However, the physiological function of KLF2 on neuronal differentiation has not been explored yet. The current study is undertaken to understand how neuronal differentiation of DPSC affects the basal level of KLF2 and how altered expression of KLF2 regulates the basal level of autophagy and mitochondrial functions. Our findings might allow us to develop a strategy by manipulating the level of KLF2 during neurogenesis, which aids in existing approaches for regenerative therapies for neurodegenerative diseases.

Materials And Method

Neural differentiation of DPSC

DPSC (P2-P7) were grown on a 60 mm tissue culture plate in minimum essential medium eagle (MEME) (Sigma Aldrich, St. Louis, MO, USA, #M8042) with 20% FBS (Peak Serum, Wellington, CO, USA, #PS-FB3), 1% anti-anti (Fisher Scientific, Gibco, Waltham, MA, USA, #15240) and 1% glutamine (Fisher Scientific, Gibco, Waltham, MA, USA, #25030081) for 48 h at 37°C in an atmosphere of 5% CO_2 in a humidified incubator. To induce neural differentiation (ND), DPSC were trypsinized and cultured into a 60 mm plate with an appropriate ND media (Fisher Scientific, Waltham, MA, #SH30893.02) supplemented with 2% FBS, 1% anti-anti, and 1% glutamine at 37°C in an atmosphere of 5% CO_2 in a humidified incubator for 10 days. The medium was replaced every third day.

KLF2 sufficiency and KLF2 deficiency

To overexpress the KLF2, DPSC were cultured in MEME with 2.5 μM of KLF2-inducer GGTI-298 (Sigma Aldrich, St. Louis, MO, USA, #G5169). After 24 h, the MEME medium was replaced by NDM with GGTI-298. The reduction of KLF2 was performed with 10 μM of KLF2 inhibitor Geranylgeranyl pyrophosphate (GGPP, Sigma Aldrich, St. Louis, MO, USA, #G6025). DPSC were cultured in NDM with GGPP for 7 days at 37°C in a CO_2 incubator. The old medium was replaced by a fresh medium every third day.

qRT-PCR analysis

The total RNA was extracted using TRIzol reagent, and the RNA concentration was detected by NanoDrop 8000 (Thermo Scientific). One μg of total RNA for each sample was reversed transcribed with a cDNA kit (Thermo Fischer Scientific, Waltham, MA, USA, #4387406) following the manufacturer's instruction. Then, cDNA was amplified with SYBR Green PCR (Thermo Fischer Scientific, Waltham, MA, USA, #4309155) by a thermal cycler PCR instrument (CFX96 Real-Time System, Bio-Rad Laboratories, Hercules, USA). The cycling parameters were as follows: initial hold at 95°C for 10s, 40 cycles at 95°C for 15s, 60°C for the 60s, then 65°C for 15s and 95°C for 50s. Relative target transcripts expression was analyzed by normalizing the calculated Ct values (threshold cycle) of target genes with internal control, GAPDH. All primer sets of target genes used in this study are included in Table S1.

Western blot analysis

Each group of cells was lysed in pre-cooled RIPA buffer (Millipore Sigma Aldrich Corporation, Burlington, MA, USA, #20–188), supplemented with protease and phosphatase inhibitors (Thermo Scientific, Waltham, MA, USA #78441) for 30 min on ice. The cell lysate was collected by centrifugation at 13,200×*g* for 15 min, and total cell protein concentration was quantified with a precision red advanced protein assay kit (Cytoskeleton Inc., Denver, CO, USA, #ADV02). An equal amount of protein (30 μg) for each sample and protein marker (Millipore Sigma Aldrich Corporation, Burlington, MA, USA, #GERPN800E) was loaded on 8–12% SDS-PAGE gels. Proteins were separated electrophoretically and then transferred to a nitrocellulose membrane (Bio-Rad Laboratories, Hercules, CA, USA, #1620115). The nitrocellulose membrane was then blocked with 5% non-fat skim milk or 5% bovine serum albumin (BSA, Sigma Aldrich Corporation, St. Louis, MO, USA, #A7906) for 2 h at room temperature. After blocking, membranes were incubated overnight with primary antibody diluted in 5% BSA (dissolved in Tris-buffered saline with 0.1% Tween 20 detergent, TBST, Boston Bioproducts, Milford, MA, USA, #IBB-180) at 4°C. The membrane was

washed thrice with TBST for 10 min each and re-incubated in species-specific horseradish peroxidase (HRP) conjugated secondary antibodies for 1 h at room temperature. Afterward, the membrane was re-washed and exposed to an enhanced chemiluminescence substrate (Amersham Pharmacia Biotechnology, Amersham, UK, #RPN2232). The protein bands were visualized and band intensity was normalized to the internal control, GAPDH using Image J software (National Institutes of Health, Bethesda, MD, USA). Details of primary antibodies are mentioned in Table S2.

Immunocytochemistry

DPSC were plated at 2×10^3 cells/well in a 6-well plate and incubated for seven days in a CO_2 incubator at 37°C. Afterward, the culture media was aspirated, and cells were washed three times with phosphate-buffered saline (PBS), followed by fixed with 4% PFA (Santa Cruz Biotechnology, ChemCruz, Dallas, TX, USA, #sc-281692) for 20 min at room temperature (RT). The cells were then permeabilized with 0.3% Triton X100 (Sigma Aldrich, St. Louis, MO, USA, #T9284) and 1% BSA in PBS (pH 7.4) for 10 min and probed with Primary antibodies (Details given in Table S2) overnight at 4°C after blocking with 5% BSA and 0.3% Triton X100 in PBS for 1 h. The following day, the cells were washed thrice with PBS for 5 min each and incubated in the dark with goat anti-rabbit/mouse conjugated with Alexa 488/649 (1:1000) for 1 h at RT. The cells were re-washed and mounted with DAPI (Invitrogen, Thermo Scientific, Waltham, MA, USA #P36931). Images were captured and analyzed by using a DMI8 inverted super-resolution confocal microscope (Leica Stellaris 8 Falcon STED).

Cellular bioenergetics analysis

The oxygen consumption rate (OCR, mitochondrial respiration) and extracellular acidification (ECAR, glycolysis) were measured during ND of DPSC using an XF24 *Extracellular Flux Analyzer* (Seahorse Bioscience, Billerica, MA, USA). In brief, differentiated cells were dissociated and re-seeded in the XF 24-well cell culture microplate (Seahorse Bioscience, Copenhagen, Denmark) at the cell density of (3×10^4) for 24 h with 1 mL of respective media for each condition. At the same time, a sensor cartridge in Seahorse XF calibrant was hydrated at 37°C in a non-CO_2 incubator overnight. On the day of Seahorse analysis, the culture was washed twice with XF base media supplemented with pyruvate, glutamine, and glucose, and all wells were filled with 500 µl of the medium/well. Then plates were incubated in a non-CO_2 incubator at 37°C for 1 h. After that, Seahorse XF calibrant was supplemented with the ATP synthase inhibitor, oligomycin (1.5 µM), uncoupler carbonyl cyanide-4-(trifluoromethoxy) phenylhydrazone (FCCP, 1 µM), complex III inhibitor rotenone, and antimycin A (0.5 µM) and then first calibrated the instrument using Seahorse Wave software 2.6.1. The calibrant plate was then replaced with an XF 24-well cell culture microplate, and oxygen consumption rate (OCR) was measured in terms of ATP turnover, maximal respiration, and reserve respiratory capacity. To perform the glycolysis stress test, we sequentially administered glucose (1 mM), oligomycin (1 µM), and 2-deoxyglucose (10 mM). ECAR parameters were calculated using Seahorse Wave software 2.6.1.

Mitochondrial ROS analysis

Cellular mitochondrial reactive oxygen species (ROS) generation was estimated using the MitoSOX red compound (Thermo Scientific, Waltham, MA, USA #M36008). Non-fluorescence MitoSOX red oxidized with mitochondrial superoxide's free radicals and produce red fluorescence. In Brief, DPSC (2×10^3) were seeded on a six-well plate overnight. Next, the medium was replaced by the NDM and incubated for 7 days. After incubation, cells were washed with 1× PBS and incubated in a 5 μM working solution prepared in Hanks' balanced salt solution (HBSS) of the MitoSOX red for 15 min at 37°C. After washing with 1× PBS, the images of cells were captured and analyzed using Leica Stellaris 8 Falcon STED confocal microscope at excitation and emission of 510/588 nm.

Cellular ROS analysis

Intracellular ROS generation was evaluated by 2',7'-dichlorodihydrofluorescein diacetate (DCFDA, Sigma Aldrich, St. Louis, MO, USA, #4091-99-0). Intracellular ROS reacts with non-fluorescent DCFDA and converts it into fluorescence molecules. In short, DPSC (2×10^3) were seeded on a six-well plate for overnight. Next, the medium was replaced by a ND medium and incubated for 7 days. After incubation, cells were washed with 1× PBS and incubated in a 5 μM working solution (prepared in PBS of the DCFDA) for 20 min at 37°C. After washing with 1× PBS, the images of cells were captured and analyzed using Leica Stellaris 8 Falcon STED confocal microscope at excitation of 495 nm and emission of 529 nm.

Statistical analysis

Statistical analysis was performed using Graph Pad Prism 5.0 (Graph Pad Software, San Diego, CA, USA) by implementing the one-way analysis of variance (ANOVA). Tukey's multiple comparisons test and Dunnett's multiple comparison test were used for comparing multiple groups. All results are expressed as mean ± standard error of the mean (SEM).

Results

Effect of neural differentiation of DPSC on KLF2, autophagy, mitophagy, and Wnt signaling molecules

To investigate whether DPSC exhibit their efficacy to differentiate into neural lineages, we cultured DPSC with neural differentiation-specific media and investigated the morphological changes that occurred during ND of DPSC on day 7 using a bright field microscope. Undifferentiated DPSC exhibited spindle-shaped morphology while differentiated cells showed neural-like pyramidal shape with short dendrite projections and a longer projection similar to the axon (Fig. 1A). Next, we examined the expression of neural-specific marker molecules like MAP2, GFAP, SYN1, and TUJ1 after induction of ND using immunocytochemistry staining (Fig. 1a). The results showed that the number of TUJ1-positive cells was hiked after induction of ND. Almost all differentiated cells were positive for MAP2, SYN1, GFAP, and undifferentiated DPSC were negative for those markers. Real-time qPCR analysis showed that the mRNA expression of neural markers (MAP2 and SYN1) was significantly increased in a time-dependent manner during differentiation (Fig. 1b). We further confirmed the ND of DPSC using western blotting analysis and

found that the neuron-specific class III β-tubulin or TUJ1 was increased when DPSC differentiated to neuron-like cells. MAP2, a more mature neural marker than TUJ1, was also gradually expressed during differentiation (Fig. 1c and Fig. S1a). To investigate the level of KLF2 during the ND of DPSC, we found that mRNA expression and protein levels of KLF2 were significantly increased during neurogenesis of DPSC. At the same time, the genes of autophagy, BECN1, ATG5, ATG7, and LC3B were also significantly increased after 7 and 10 days of ND (Fig. 1d). The western blot analysis revealed that after 7 and 10 days of induction, the ATG5, LC3B, and Beclin1 were highly expressed. LAMP1, a lysosomal membrane maker, facilitates the successful maturation of both autophagosomes and phagosomes. Like early autophagy markers, LAMP1 expression also gradually increased during ND (Fig. 1e and Fig. S1b). We further assessed the mitochondrial dynamics markers and found that the PINK1, Parkin, DRP1, and FIS1 significantly increased after 10 days of differentiation (Fig. 1f). We determined similar trends in protein expression of Parkin and DRP1, however, FIS1 did not show remarkable differences (Fig. 1g and Fig. S1c). These data suggest that ND in DPSC might require a transcriptional regulator, KLF2, along with autophagy and mitophagy-associated genes. To get more insight into the molecular mechanism underlying the ND of DPSC, we examined the Wnt pathway-specific markers (Wnt5a, LRP6, CTNNB1 and DVL3, GSK3B). RT-PCR analysis revealed that the gene level of Wnt5a/b and LRP6 was significantly increased during ND. However, β-catenin was significantly upregulated during only the initial days of ND (Fig. 1h). In the western blot analysis, WNT5a/b and DVL3 expression were increased at 7 and 10 days of differentiation. Correspondingly, protein expression of GSK3α/β declined during differentiation. However, mRNA expression of GSK3B was dramatically increased time-dependent manner (Fig. 1i and Fig. S1d). The difference in protein and gene expression may be due to post-translational modification.

Effect of KLF2 deficiency on autophagy, mitophagy, mitochondrial dynamics, and neural differentiation of DPSC

To determine the role of KLF2 in ND, we cultured DPSC in the NDM without or with GGPP, an inhibitor of KLF2, and examined the consequences involved in neural-like cell differentiation of DPSC. We found the mRNA expression of KLF2 was marginally decreased in the presence of GGPP (ND + GGPP) compared to the neural differentiated control (ND), indicating that GGPP leads to KLF2 deficiency during neural differentiation. Concurrently, partial KLF2 deficiency led to a conspicuously decrease in the mRNA expression of neural markers, MAP2, SYN1, and NeuN, indicating that KLF2 is an essential transcription factor required for ND of DPSC (Fig. 2a). We next probed into the translational level changes of KLF2 and MAP2 in the DPSC during ND differentiation in the presence and absence of GGPP. As expected, the protein expression of KLF2 and MAP2 was decreased in ND + GGPP group compared to the ND group (Fig. 2b and Fig. S2). We also performed immunocytochemistry to detect the expression level of MAP2 and TUJ1. We found that MAP2 expression, correlating to transcription data, was significantly decreased in the presence of GGPP compared to the ND group. TUJ1 expression was strikingly increased in the ND group and restored to the basal level of DPSC (Fig. 2c, 2d). Subsequently, the effect of KLF2 deficiency on the morphology of neural-like cell differentiation was assessed using bright field microscopy. We analyzed the soma area and neurite growth in the obtained images using ImageJ software. As shown in

the graphs (Fig. 2e, 2f), an insignificant difference between groups was observed suggesting that partial KLF2 deficiency only suppresses the ND at the transcriptional and translational levels.

We next examined the effect of KLF2 deficiency on autophagy during ND. We observed that the mRNA expression level of autophagy markers (ATG7, BCEN1, and LC3B) was strongly decreased after partial KLF2 deficiency (Fig. 3a). In the western blot analysis, we found that the protein expression level of ATG5, LC3B, and LAMP1 was also decreased after the ND treated with GGPP (Fig. 3b and Fig. S3), indicating that KLF2 plays a vital role in the autophagy process. Immunofluorescences analysis of ATG5 and LC3B was strongly corroborating with western blot analysis. Likewise, mitophagy is essential for ND to eliminate the damaged mitochondria. So, we next wanted to investigate how the limited expression of KLF2 affects the transcriptional and translational of mitophagy-associated markers. The transcript level of PINK1 was marginally decreased in the ND with GGPP, while the gene expression of Parkin was strikingly decreased after the deficiency of KLF2 compared to ND (Fig. 3a). Corroborating to transcription data, the protein expression of Parkin in the ND with GGPP was remarkably decreased. In contrast, the protein expression of DRP1 was slightly downregulated in the GGPP-treated ND group (Fig. 3b and Fig. S3). Next, we performed immunocytochemistry to visualize the protein expression of ATG5, LC3B, PINK1, and Parkin. As anticipated, ATG5, LC3B, PINK1, and Parkin expression in DPSC and KLF2-deficient neural differentiated cells were approximately similar while increased during the ND (Fig. 3c, 3d). Our data indicate that KLF2 is essential to regulating mitophagy during ND of DPSC. We also determined whether KLF2 deficiency alters Wnt signaling during ND. We observed a significant transcriptional decrease in Wnt5a and DVL3 levels in KLF2-deficient neural differentiated cells. Western blot analysis represents that a marginal reduction in protein expression of Wnt5a and DVL3 (Fig. 3a and Fig. S3).

Next, we investigated the intracellular reactive oxygen species (ROS) generation and mitochondrial superoxide generation by MitoSOX and DCFDA staining after NDs for 7 days because ROS acts as a signaling stimulator for cellular pathways. We found that differentiated neuron-like cells showed a significant decrease in ROS and mitochondria superoxide production compared to DPSC. After the KLF2 deficiency, ROS and superoxide production was found to be shifted towards the basal level (Fig. 4a, 4b). To investigate the mitochondrial functions, we examined the mitochondrial oxygen consumption rate (OCR) in basal respiration, mitochondrial respiration, spare respiration capacity conditions, and ATP production. The basal respiration and ATP production was significantly decreased in the neural differentiated control group compared to the undifferentiated control group. In contrast, an insignificant difference was observed between GGPP-treated ND and ND Control group. A significant hike in maximum respiration and spare respiration capacity during ND of DPSC was detected while GGPP slightly shifted such mitochondrial metabolism effect towards DPSC (Fig. 4c and Fig. S6a). We next sought to examine the extracellular acidification rate defining the glycolytic metabolism during ND. We found that the neural differentiating cells catabolize the glucose through the glycolysis pathway to fulfill energy demand in the absence of glutamine. The non-glycolytic acidification, glycolysis, glycolysis capacity, and glycolytic reserve were significantly hiked in neuronal-like differentiated cells, however, partial KLF2-deficient neural-like differentiated cells exhibited less non-glycolytic acidification and glycolysis (Fig. 4d and Fig. S6b).

Effect of KLF2 overexpression on autophagy, mitophagy, mitochondrial dynamics, and neural differentiation of DPSC

Next, we focused on defining how KLF2 regulates neural differentiation; to do so, we stimulated DPSC with KLF2 inducer GGTI-298 and cultured it with ND medium (NDM) for 7 days. We found that the GGTI-298-treated DPSC were differentiated to neural-like cells, and showed higher KLF2 expression than cells differentiated in only the NDM. The mRNA expression of MAP2 and SYN1 was also markedly increased in the presence of GGTI-298. NeuN expression was increased only after the addition of GGTI-298, indicating KLF2 overexpression accelerated ND rate (Fig. 5a). Western blot analysis showed that expression of KLF2 was increased when GGTI-298 was added to NDM. Consistently, the protein expression of MAP2 and TUJ1 was also marginally increased in KLF2 overexpressed group (Fig. 5b and Fig. S4). Next, we performed the immunostaining for MAP2 and TUJ1, and image intensity analysis revealed that overexpression of KLF2 induced neuronal differentiation rate compared to ND control (Fig. 5c, 5d). Subsequently, we observed that the overexpression of KLF2 increased marginally soma area and neurite growth compared to ND, indicating that KLF2 overexpression induces the rate of ND (Fig. 5e and 5f).

To further determine the function of KLF2 on autophagy during ND, we examined the alteration of transcriptional and translational in autophagy-associated markers after KLF2 overexpression. A slight increase in the transcript level of ATG5, ATG7, and LC3B was determined in KLF2-overexpressed neural differentiated cells compared to differentiated neural cells (Fig. 6a). Corroborating to mRNA level, western blot analysis for autophagosome markers (ATG5, LC3B, and Beclin1) and autolysosome marker (LAMP1) collectively revealed that KLF2 overexpression promotes marginal autophagy and facilitates neuronal differentiation (Fig. 6b and Fig. S5). We further wanted to investigate how KLF2 overexpression affects mitophagy during ND. Similar to autophagy, KLF2 overexpression slightly increased the mRNA expression of mitophagy-associated genes, PINK1, Parkin, FIS1, and DRP1, compared to normal ND (Fig. 6a). We further examined whether these effects were consistent with the translational level. We performed western blot analysis for Parkin and DRP1 and observed that Parkin expression was significantly increased compared to the ND group, while DRP1 expression persisted the same in both groups (Fig. 6b and Fig. S5). In the immunostaining analysis for ATG5, LC3B, PINK1, and Parkin, a dramatically increased in protein expression was detected in KLF2 overexpressed differentiated neural cells compared to neural differentiated cells (Fig. 6c and 6d).

Next, we wanted to examine the effect of KLF2 overexpression on intracellular ROS generation and mitochondrial superoxide production. An insignificant difference between the ND group and the ND + GGTI-298 group was observed in ROS production determined by MitoSOX and DCFDA staining (Fig. 7a and 7b). To investigate the mitochondrial functions, we analyzed that the addition of GGTI-298 in ND media strikingly reduces the basal respiration and ATP production of differentiated cells, indicating the neuronal-like differentiated cells may be shifted towards maturation (Fig. 7c and Fig. S7a). Similarly, in ECAR analysis, non-glycolytic acidification was reduced compared to neuronal-like differentiated cells.

Though, glycolysis and glycolytic capacity were not significantly altered in ND + GGTI-298 group (Fig. 7d and Fig. S7b).

Discussion

The replacement of degenerated neurons with pre-differentiated neural-like stem cells appears to be a promising stem cells-based therapy for neurodegenerative disorders (7). Dental-pulp-derived mesenchymal stem cells (DPSC) are highly prolific in differentiating towards multiple lineages, chondrocytes, adipocytes, neurons, and osteoblast cells in the presence of appropriate signals (8, 10). Additionally, DPSC possess inherent immunomodulatory and neuroprotective properties (4, 5). Therefore, they have been subjected to clinical studies to cure neurodegenerative disorders more effectively. The molecular changes that occur during ND of DPSC remain unclear. Autophagy and mitophagy play a vital role during the proliferation and differentiation of stem cells. Autophagy-associated pathways cross-talk with KLF2, one of the kruppel-like transcription factors (KLFs) belonging to the zinc finger family, to maintain intracellular homeostasis (35). The molecular function and expression level of KLF2 under healthy physiological and pathological conditions differs. For instance, we previously showed that upregulated KLF2 positively regulates autophagy during osteoblastic differentiation. Conversely, we also demonstrated that KLF2 expression is reduced during the osteoclastogenic differentiation of myeloid cells and negatively regulates autophagy (31). A recent study reported that the KLF2 exhibits a protective role in neonatal hypoxic-ischemic brain injury in rats by increasing the expressions of the downstream signaling molecules IRF4 and HDAC7 (36). These findings create a curiosity about how KLF2 regulates the molecular changes during neurogenesis. ND of stem cells requires a much higher level of autophagy and mitophagy than the basal level of stem cells to meet the cellular nutrition and energy demands, as evident by previous studies (24). However, the expression level and role of KLF2 during ND of DPSC have not been explored yet. The current study focuses on defining the molecular involvement of KLF2 during ND of DPSC, which will provide a new molecular target for developing a treatment option for neurodegenerative diseases.

In this study, we first confirmed the neurogenic differentiation efficacy of DPSC using qRT-PCR, western blot analysis, and immunocytochemistry. Our findings showed that the expression of early and mature neural markers, MAP2, TUJ1, synapsin, and GFAP was gradually increased in a time-dependent manner during ND, indicating the supplemented signals in ND media efficiently induce the commitment of DPSC towards ND. Our findings showed that both autophagy and mitophagy increased during the ND of DPSC, as confirmed by the upregulated level of autophagy markers, LC3B, BECN1, ATG5, ATG7, and LAMP1, and mitophagy markers, PINK1, Parkin, DRP1, and FIS1 indicating that the autophagy and mitophagy are essential for the ND. In consistent with our study, recent studies described that autophagy inducer, 5-Azacytidine enhances the neuronal differentiation of human placenta-derived mesenchymal stem cells. (26). Interestingly, we found that KLF2 expression was increased during the ND of DPSC time-dependently. To further investigate the principal function of KLF2 on ND, we performed KLF2 deficiency, which slows down the efficacy of DPSC towards neuron-like cells. GGPP, an isoprenoid metabolite, regulates various cell-signaling pathways, including autophagy. Previous studies reported that deletion of

GGPP triggers autophagy (37) and the addition of GGPP to cerivastatin-treated HUVEC significantly reduced elevated-KLF2 expression (38). These findings represent that KLF2 deficiency may affect autophagy and mitophagy during ND of DPSC. Therefore, we are further motivated to investigate how KLF2 deficiency affects autophagy and mitophagy during the ND of DPSC. KLF2 deficiency exhibited a positive correlation in the reduction of autophagy markers (LC3B, ATG5, and LAMP1) and mitophagy markers (PINK1, Parkin, DRP1, FIS1) along with ND marker molecules (MAP2, TUJ1). This study corroborated previous studies in which siRNA-mediated knockdown of KLF2 reduces the autophagy and osteoblast differentiation of DPSC (39). Previous studies demonstrated that GGTI-298 inhibits the protein geranylgeranylation, and subsequently induces significantly the KLF2 expression. (38). So, we next performed the experiment with KLF2 overexpression using KLF2 inducer and reconfirmed that the KLF2 overexpression increased ND by enhancing autophagy and mitophagy. This finding indicates that KLF2 is an essential transcription factor in modulating autophagy and mitophagy responses during the ND of DPSC.

Additionally, we found that the Wnt signaling pathway markers, Wnt5a and DVL3, were elevated during ND of DPSC. Our findings support an earlier observation of ND and development involving the activation of the Wnt5a pathway (40). It was also reported that autophagy pathways interplay with Wnt5a signaling pathways and regulate each other through a positive feedback mechanism, as both pathways are essential for stem cell differentiation (8, 41). Next, we confirmed the involvement of Wnt5a pathway markers after KLF2 knockdown and overexpression experiments. A significant drop in Wnt5a and DVL3 expression was observed after KLF2 knockdown, indicating that autophagy positively regulates the Wnt5a pathways during ND.

Mitochondria critically regulate the metabolic reprogramming of stem cells during neuronal differentiation (42). Specifically, it regulates several essential cellular processes, including reactive oxygen species (ROS) signaling, calcium signaling, apoptosis, and maintaining cellular homeostasis. Recent studies demonstrate that mitochondria govern the cell fate during neurogenesis (43). Most importantly, mitochondria are the cell's powerhouse, providing energy during the differentiation of cells through oxidative phosphorylation (44). Therefore, it is essential to understand how mitochondrial bioenergetics are affected during the neuronal differentiation of DPSC and the role of KLF2 in this process. An increase in mitochondrial respiration and spare respiratory capacity was observed in differentiated neuron-like cells after 7 days, indicating that differentiated DPSC switches their metabolism towards oxidative phosphorylation, which is in support of previous studies (45). When GGTI-298 accelerates neuronal differentiation of DPSC, a reduction in ATP production and mitochondrial activity was observed. This data is corroborated by a previous study showing the reduced ATP demand and mitochondrial activity in ND of human embryonic stem cells (46). Since GGPP limits neuronal differentiation, maximum respiration and spare respiratory capacity were only reduced but not reached to DPSC's metabolism. Moreover, GGPP-mediated KLF2 deficiency did not alter the ATP production, indicating partial deficiency of KLF2 inefficiently affects mitochondrial respiration. Such metabolic reprogramming in differentiated neuron-like cells motivated us to examine the extracellular acidification rate, which represents the glycolytic activity of the cells. Neuronal-like differentiated cells demand high

glucose to support the biosynthesis essential for neurite outgrowth and synapse formation (47). Here, neuron-like differentiated cells showed higher glycolytic capacity, which is confirmed by observing the reduction in ATP production after the addition of glucose analog, 2-DG. Our finding indicates that neuron-like differentiated cells exhibit metabolic flexibility, i.e., differentiated cells can switch between both cellular bioenergetics, glycolysis, and mitochondrial respiration. For instance, in the presence of glucose only, differentiating cells would fulfill their energy demands through glycolysis because the balance between glycolysis and mitochondrial respiration is essential for stem cell differentiation (48). GGPP-mediated KLF2 deficiency reduces extracellular acidification, which is consistent with our data. Taken together, our data established that KLF2 regulates autophagy, mitophagy pathways, and metabolic reprogramming during ND of DPSC.

Conclusion

In summary, we provide the first evidence of the induction of KLF2 during ND of DPSC, which positively regulates the autophagy and mitophagy pathways. We verified that KLF2-mediated autophagy and mitophagy control the ND of DPSC using chemical-mediated partial loss-of-function and gain-of-function approaches for the KLF2 gene. Our results show that KLF2 functions as a modulator of autophagy and mitophagy processes during neurogenesis. The current study unravels a strategy for targeting KLF2 that could be used to develop a new potential regenerative therapeutic approach for neurogenerative disorders.

Declarations

Funding

This work was supported in part by National Institutes of Health grants, R01AR068279 (NIAMS), STTR R42EY031196 (NEI), and STTR 1R41AG057242 (NIA). The funders had no role in the study design, data collection, and analysis, decision to publish, or preparation of the manuscript.

Author contributions

All authors were involved in drafting the article or revising it critically for important intellectual content, and all authors approved the final version to be published. Study conception, design, and manuscript writing: PP and HD. Acquisition of data: PP, PN, MD, DB Analysis and interpretation of data: PP and HD.

Declaration of competing interest

Authors do not have any potential conflict of interest to disclose.

References

1. Gao HM, Hong JS. Why neurodegenerative diseases are progressive: uncontrolled inflammation drives disease progression. Trends Immunol. 2008;29(8):357–65.
2. Lindvall O, Kokaia Z, Martinez-Serrano A. Stem cell therapy for human neurodegenerative disorders–how to make it work. Nature medicine. 2004;10(7):S42-S50.
3. Joyce N, Annett G, Wirthlin L, Olson S, Bauer G, Nolta JA. Mesenchymal stem cells for the treatment of neurodegenerative disease. Regenerative medicine. 2010;5(6):933–46.
4. Reboussin É, Buffault J, Brignole-Baudouin F, Goazigo R-L, Riancho L, Olmiere C, et al. Evaluation of neuroprotective and immunomodulatory properties of mesenchymal stem cells in an ex vivo retinal explant model. Journal of neuroinflammation. 2022;19(1):1–17.
5. Kim YJ, Park HJ, Lee G, Bang OY, Ahn YH, Joe E, et al. Neuroprotective effects of human mesenchymal stem cells on dopaminergic neurons through anti-inflammatory action. Glia. 2009;57(1):13–23.
6. Giacomelli E, Vahsen BF, Calder EL, Xu Y, Scaber J, Gray E, et al. Human stem cell models of neurodegeneration: from basic science of amyotrophic lateral sclerosis to clinical translation. Cell Stem Cell. 2022;29(1):11–35.
7. Puranik N, Arukha AP, Yadav SK, Yadav D, Jin JO. Exploring the role of stem cell therapy in treating neurodegenerative diseases: Challenges and current perspectives. Current Stem Cell Research & Therapy. 2022;17(2):113–25.
8. Rolph DN, Deb M, Kanji S, Greene CJ, Das M, Joseph M, et al. Ferutinin directs dental pulp-derived stem cells towards the osteogenic lineage by epigenetically regulating canonical Wnt signaling. Biochim Biophys Acta Mol Basis Dis. 2018:165314.
9. Ledesma-Martínez E, Mendoza-Núñez VM, Santiago-Osorio E. Mesenchymal stem cells derived from dental pulp: a review. Stem cells international. 2016;2016.
10. Lan X, Sun Z, Chu C, Boltze J, Li S. Dental pulp stem cells: an attractive alternative for cell therapy in ischemic stroke. Frontiers in neurology. 2019;10:824.
11. Mortada I, Mortada R, Al Bazzal M. Dental pulp stem cells and the management of neurological diseases: an update. Journal of Neuroscience Research. 2018;96(2):265–72.
12. Heng BC, Lim LW, Wu W, Zhang C. An overview of protocols for the neural induction of dental and oral stem cells in vitro. Tissue Engineering Part B: Reviews. 2016;22(3):220–50.
13. Wang F, Jia Y, Liu J, Zhai J, Cao N, Yue W, et al. Dental pulp stem cells promote regeneration of damaged neuron cells on the cellular model of Alzheimer's disease. Cell Biology International. 2017;41(6):639–50.
14. Sharma Y, Shobha K, Sundeep M, Pinnelli VB, Parveen S, Dhanushkodi A. Neural Basis of Dental Pulp Stem Cells and its Potential Application in Parkinson's disease. CNS & Neurological Disorders-Drug Targets (Formerly Current Drug Targets-CNS & Neurological Disorders). 2022;21(1):62–76.
15. Mead B, Logan A, Berry M, Leadbeater W, Scheven BA. Concise review: dental pulp stem cells: a novel cell therapy for retinal and central nervous system repair. Stem Cells. 2017;35(1):61–7.

16. Abeysinghe HC, Bokhari L, Quigley A, Choolani M, Chan J, Dusting GJ, et al. Pre-differentiation of human neural stem cells into GABAergic neurons prior to transplant results in greater repopulation of the damaged brain and accelerates functional recovery after transient ischemic stroke. Stem Cell Res Ther. 2015;6:186.
17. Bonaventura G, Munafo A, Bellanca CM, La Cognata V, Iemmolo R, Attaguile GA, et al. Stem Cells: Innovative Therapeutic Options for Neurodegenerative Diseases? Cells. 2021;10(8).
18. Osathanon T, Sawangmake C, Nowwarote N, Pavasant P. Neurogenic differentiation of human dental pulp stem cells using different induction protocols. Oral diseases. 2014;20(4):352–8.
19. Chang C-C, Chang K-C, Tsai S-J, Chang H-H, Lin C-P. Neurogenic differentiation of dental pulp stem cells to neuron-like cells in dopaminergic and motor neuronal inductive media. Journal of the Formosan Medical Association. 2014;113(12):956–65.
20. Heng BC, Jiang S, Yi B, Gong T, Lim LW, Zhang C. Small molecules enhance neurogenic differentiation of dental-derived adult stem cells. Archives of oral biology. 2019;102:26–38.
21. Chang NC. Autophagy and stem cells: self-eating for self-renewal. Frontiers in Cell and Developmental Biology. 2020;8:138.
22. Onishi M, Yamano K, Sato M, Matsuda N, Okamoto K. Molecular mechanisms and physiological functions of mitophagy. The EMBO journal. 2021;40(3):e104705.
23. Lin Q, Chen J, Gu L, Dan X, Zhang C, Yang Y. New insights into mitophagy and stem cells. Stem cell research & therapy. 2021;12(1):1–14.
24. Fleming A, Rubinsztein DC. Autophagy in neuronal development and plasticity. Trends in neurosciences. 2020;43(10):767–79.
25. Doxaki C, Palikaras K. Neuronal mitophagy: friend or foe? Frontiers in cell and developmental biology. 2021;8:611938.
26. Sotthibundhu A, Muangchan P, Phonchai R, Promjantuek W, Chaicharoenaudomrung N, Kunhorm P, et al. Autophagy promoted neural differentiation of human placenta-derived mesenchymal stem cells. in vivo. 2021;35(5):2609–20.
27. Das H, Kumar A, Lin Z, Patino WD, Hwang PM, Feinberg MW, et al. Kruppel-like factor 2 (KLF2) regulates proinflammatory activation of monocytes. Proc Natl Acad Sci U S A. 2006;103(17):6653–8.
28. Rolph D, Das H. Transcriptional Regulation of Osteoclastogenesis: The Emerging Role of KLF2. Front Immunol. 2020;11:937.
29. Jha P, Das H. KLF2 in Regulation of NF-kappaB-Mediated Immune Cell Function and Inflammation. Int J Mol Sci. 2017;18(11).
30. Sen-Banerjee S, Mir S, Lin Z, Hamik A, Atkins GB, Das H, et al. Kruppel-like factor 2 as a novel mediator of statin effects in endothelial cells. Circulation. 2005;112(5):720–6.
31. Laha D, Deb M, Das H. KLF2 (kruppel-like factor 2 [lung]) regulates osteoclastogenesis by modulating autophagy. Autophagy. 2019;15(12):2063–75.

32. Winkelmann R, Sandrock L, Porstner M, Roth E, Mathews M, Hobeika E, et al. B cell homeostasis and plasma cell homing controlled by Krüppel-like factor 2. Proceedings of the National Academy of Sciences. 2011;108(2):710-5.
33. Feinberg MW, Lin Z, Fisch S, Jain MK. An emerging role for Kruppel-like factors in vascular biology. Trends Cardiovasc Med. 2004;14(6):241–6.
34. Maity J, Barthels D, Sarkar J, Prateeksha P, Deb M, Rolph D, et al. Ferutinin induces osteoblast differentiation of DPSCs via induction of KLF2 and autophagy/mitophagy. Cell Death Dis. 2022;13(5):1–12.
35. Rolph D, Das H. Transcriptional regulation of osteoclastogenesis: the emerging role of KLF2. Frontiers in immunology. 2020;11:937.
36. Wu F, Li C. KLF2 up-regulates IRF4/HDAC7 to protect neonatal rats from hypoxic-ischemic brain damage. Cell death discovery. 2022;8(1):1–10.
37. Zhang JH. Autophagy and mitophagy in cellular damage control. Redox Biol. 2013;1(1):19–23.
38. Parmar KM, Nambudiri V, Dai G, Larman HB, Gimbrone MA, Jr., Garcia-Cardena G. Statins exert endothelial atheroprotective effects via the KLF2 transcription factor. J Biol Chem. 2005;280(29):26714–9.
39. Maity J, Deb M, Greene C, Das H. KLF2 regulates dental pulp-derived stem cell differentiation through the induction of mitophagy and altering mitochondrial metabolism. Redox Biol. 2020;36:101622.
40. Kondo T, Matsuoka AJ, Shimomura A, Koehler KR, Chan RJ, Miller JM, et al. Wnt signaling promotes neuronal differentiation from mesenchymal stem cells through activation of Tlx3. Stem cells. 2011;29(5):836–46.
41. Lorzadeh S, Kohan L, Ghavami S, Azarpira N. Autophagy and the Wnt signaling pathway: A focus on Wnt/β-catenin signaling. Biochimica et Biophysica Acta (BBA)-Molecular Cell Research. 2021;1868(3):118926.
42. Ozgen S, Krigman J, Zhang R, Sun N. Significance of mitochondrial activity in neurogenesis and neurodegenerative diseases. Neural Regeneration Research. 2022;17(4):741.
43. Brunetti D, Dykstra W, Le S, Zink A, Prigione A. Mitochondria in neurogenesis: Implications for mitochondrial diseases. Stem Cells. 2021;39(10):1289–97.
44. Kuntz EM, Baquero P, Michie AM, Dunn K, Tardito S, Holyoake TL, et al. Targeting mitochondrial oxidative phosphorylation eradicates therapy-resistant chronic myeloid leukemia stem cells. Nature medicine. 2017;23(10):1234–40.
45. Zheng X, Boyer L, Jin M, Mertens J, Kim Y, Ma L, et al. Metabolic reprogramming during neuronal differentiation from aerobic glycolysis to neuronal oxidative phosphorylation. elife. 2016;5:e13374.
46. Birket MJ, Orr AL, Gerencser AA, Madden DT, Vitelli C, Swistowski A, et al. A reduction in ATP demand and mitochondrial activity with neural differentiation of human embryonic stem cells. J Cell Sci. 2011;124(Pt 3):348–58.

47. Birket MJ, Orr AL, Gerencser AA, Madden DT, Vitelli C, Swistowski A, et al. A reduction in ATP demand and mitochondrial activity with neural differentiation of human embryonic stem cells. Journal of cell science. 2011;124(3):348–58.
48. Zhang C, Skamagki M, Liu Z, Ananthanarayanan A, Zhao R, Li H, et al. Biological significance of the suppression of oxidative phosphorylation in induced pluripotent stem cells. Cell reports. 2017;21(8):2058–65.

Figures

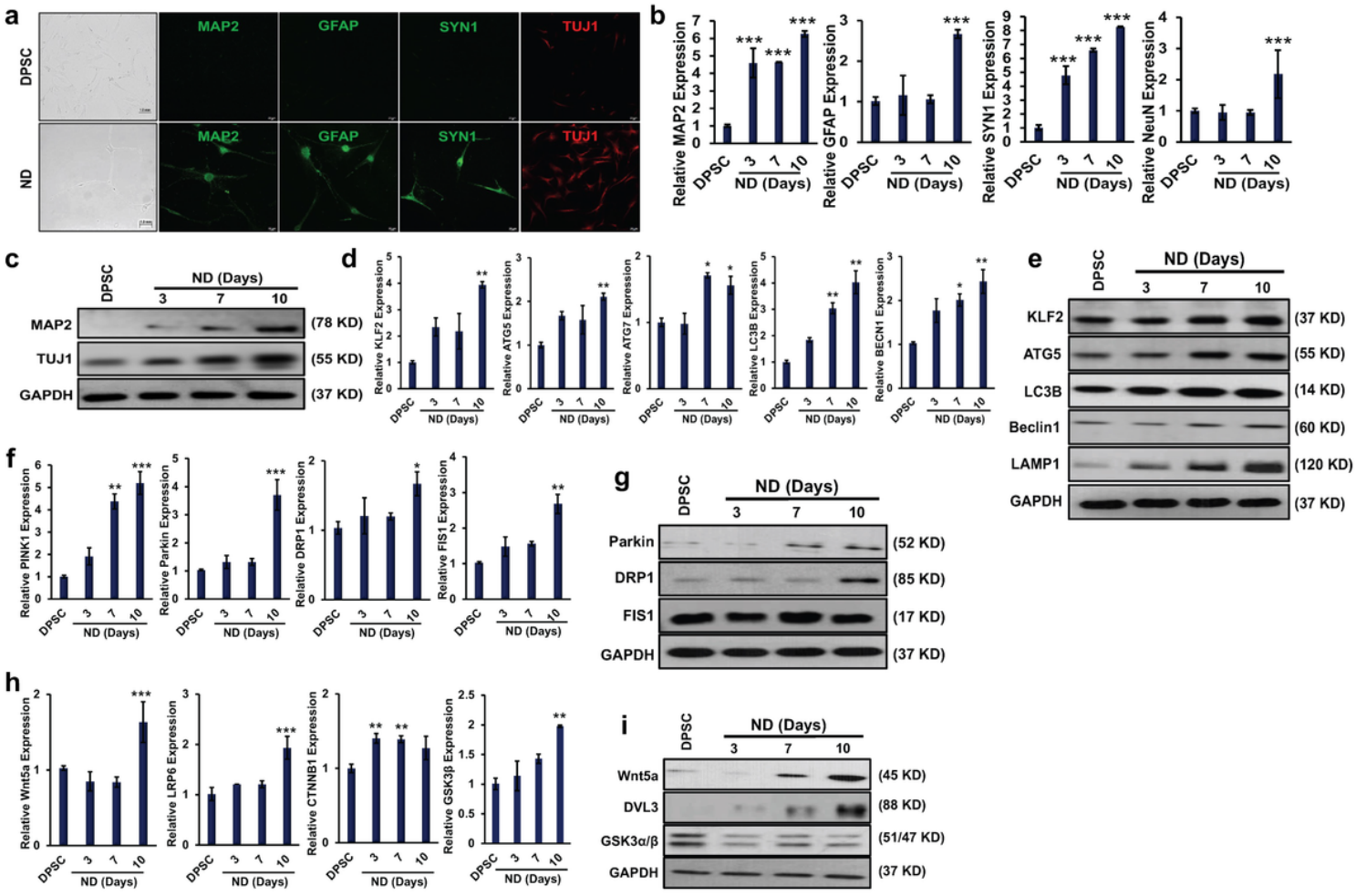

Figure 1

KLF2, autophagy, and Wnt signaling molecules were induced during neural differentiation. a. Confocal microscopy images were shown for neural markers, MAP2 (green), GFAP (green), SYN1 (green) and TUJ1 (red), in differentiated neuronal-like cells (ND) and undifferentiated DPSC. **b.** The mRNA expression level of MAP2, GFAP, SYN1, and NeuN was determined by qRT-PCR at various time points of neuronal differentiation of DPSC. Statistical significance, $p<0.001$ was shown (***) compared to DPSC controls. **c.** Western blot of MAP2 and TUJ1 on the 3, 7 and 10 days of DPSC' neuronal differentiation keeping GAPDH as an internal loading control. **d.** qRT-PCR evaluation of KLF2, autophagy-associated markers,

ATG5, ATG7, LC3B and BECN1, mitophagy-linked markers, PINK1, Parkin, DRP1 and FIS1, and Wnt signaling molecules, Wnt5a, LRP6, and CTNNB1. Statistical differences between undifferentiated DPSC and differentiated neuronal-like cells were shown as *** p<0.001, ** p<0.01, * p < 0.05. **e.** Western blot of KLF2 and autophagy markers, ATG5, LC3B, Beclin1 and LAMP1; **f.** Mitophagy markers, Parkin Drp1, FIS1; **g.** Wnt signaling pathway markers, Wnt5a, DVL3, and GSK3a/b. GAPDH was used as an internal loading control.

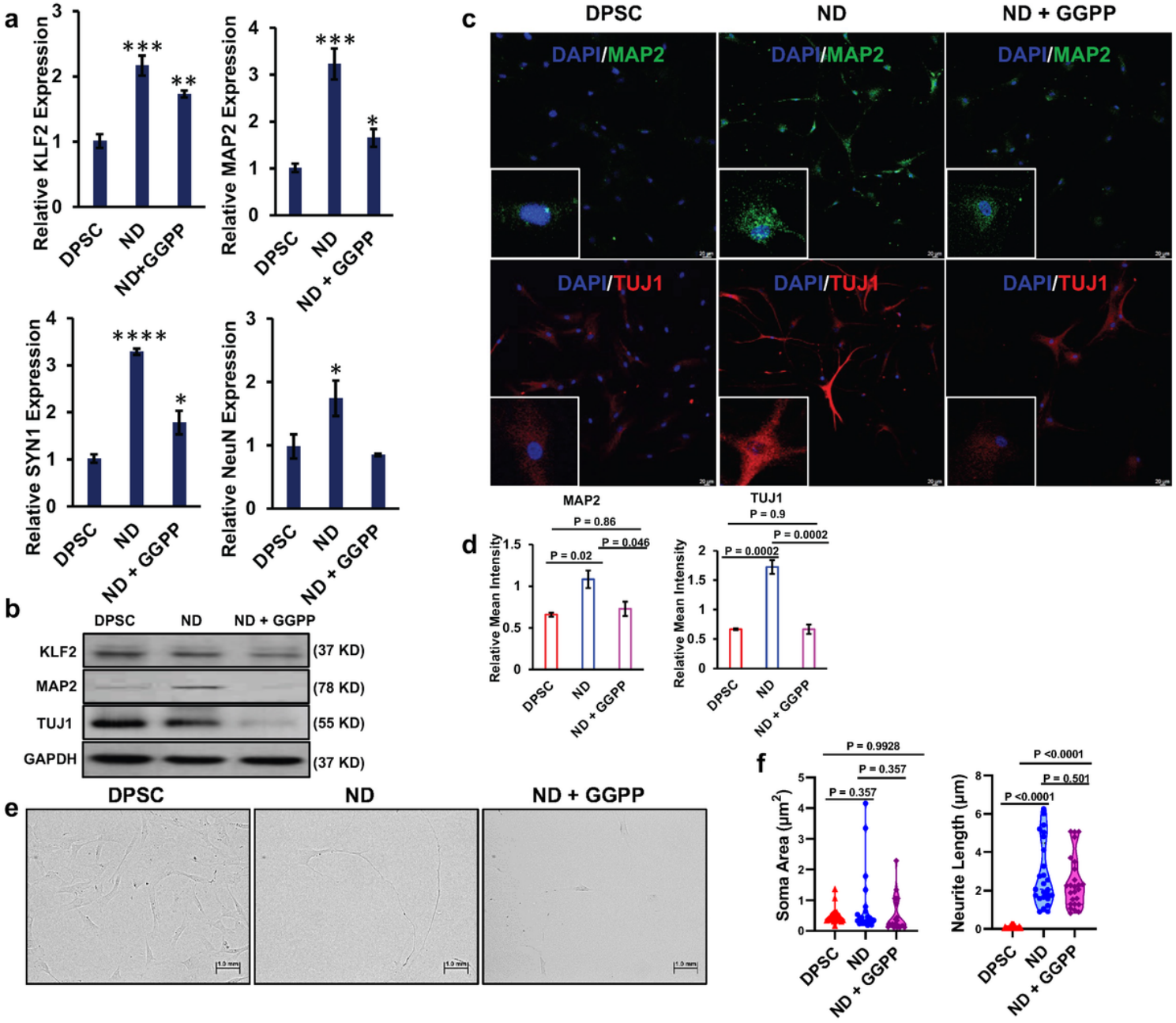

Figure 2

KLF2 deficiency reduces neuronal differentiation. a. qRT-PCR analysis of KLF2, MAP2, SYN1, and NeuN was determined in cells after ND, ND + GGPP, and DPSC. Statistical significance, *** p<0.001, ** p<0.01, * p < 0.05 compared to DPSC controls. **b.** The protein level of KLF2, MAP2, TUJ1 and GAPDH as an internal control was determined by western blot. **c**. Immunofluorescence images of MAP2 (green) and TUJ1 (red)

were shown. Inset represents a zoom view of targeted cell. **d**. Relative mean intensity of the images (n = 6). **e.** Bright-field images of cells after ND, ND + GGPP, and DPSC were shown. **f.** Graphs represent the quantitative evaluation of soma area (μm^2) and neurite length (μm) of the differentiated cells (n = 6).

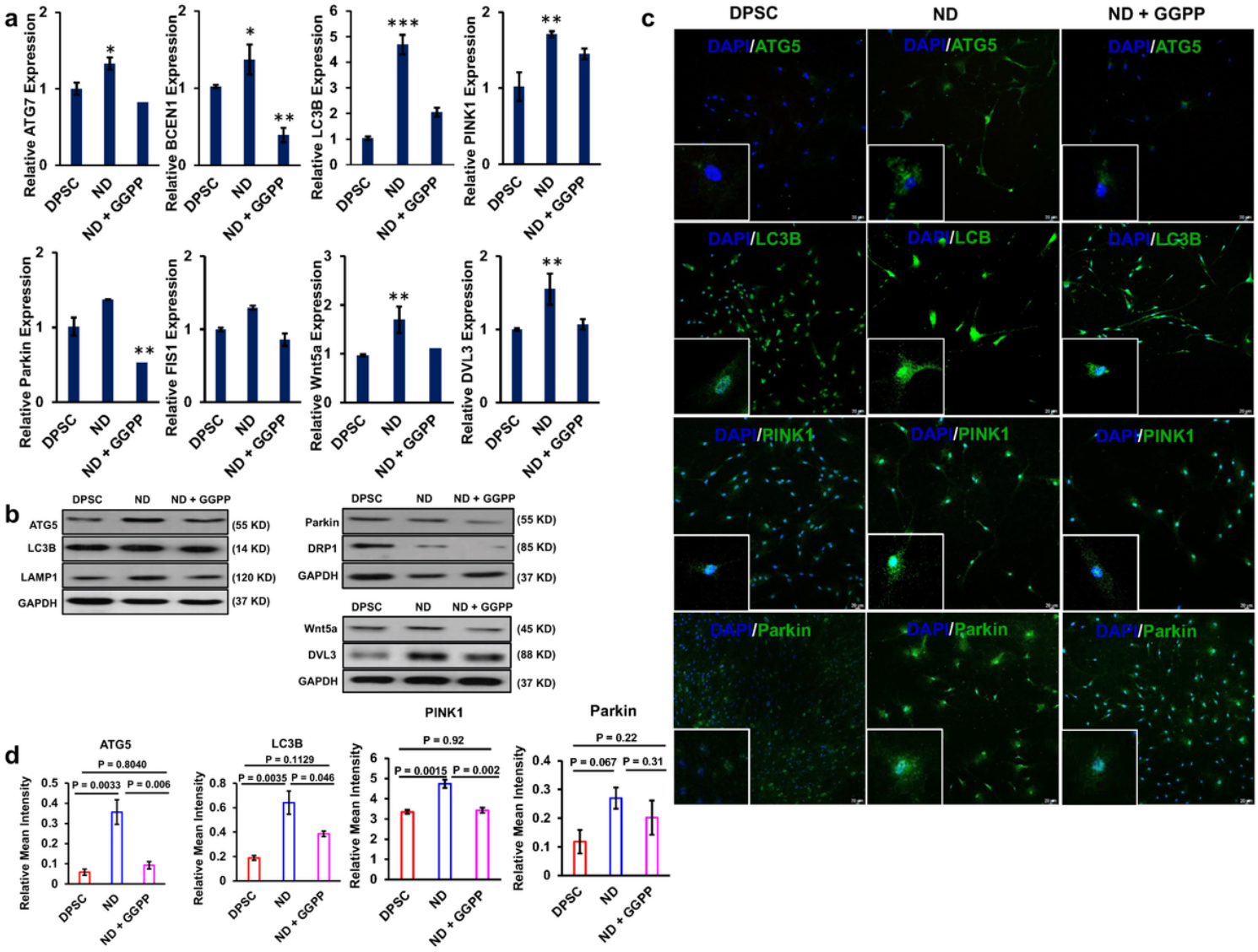

Figure 3

KLF2 deficiency suppresses autophagy, mitophagy, and Wnt signaling pathway molecules. a. qRT-PCR analysis of ATG7, BCEN1, LC3B, Parkin, PINK1, FIS1, Wnt5a, and DVL3 was determined in cells after ND, ND + GGPP, and DPSC. Statistical significance, *** p<0.001, ** p<0.01, * p < 0.05 compared to DPSC controls. **b.** The protein level of ATG7, LC3B, and LAMP1 (Left panel), Parkin1, DRP1 (right upper panel), and Wnt5a and DVL3 (right lower panel) was determined by western blot, keeping GAPDH as an internal control. **c**. Immunofluorescence images of ATG5, LC3B, PINK1, and Parkin (green) were shown. Inset represents a zoom view of targeted cell. **d**. Relative mean intensity of the images (n = 6).

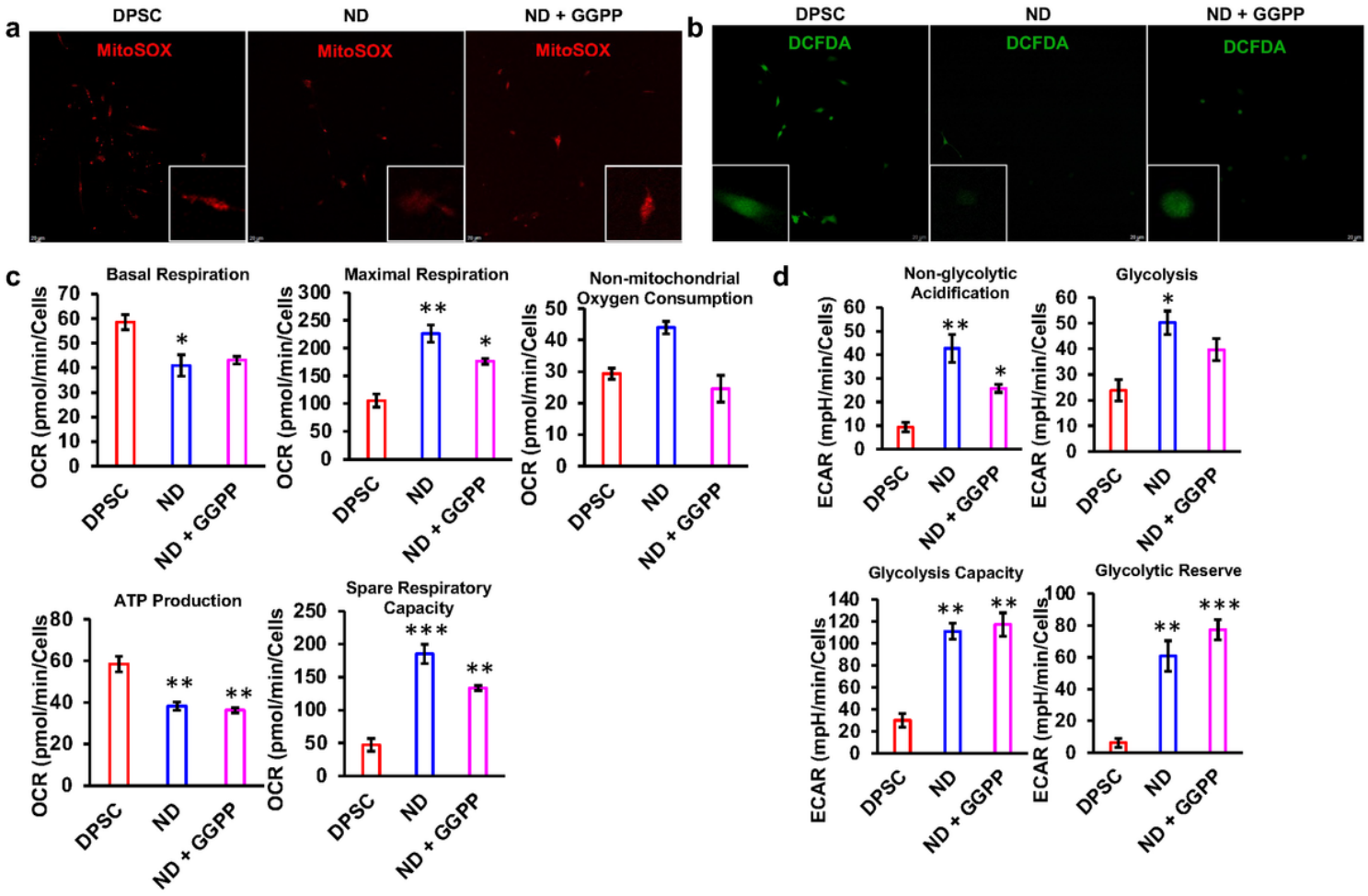

Figure 4

Effect of KLF2 deficiency on redox signaling and cellular bioenergetics. a. MitoSOX-stained cells were shown after ND, ND + GGPP, and DPSC. Inset represents a zoom view of targeted cell. **b.** DCFDA-stained cells were shown after ND, ND + GGPP, and DPSC. Inset represents a zoom view of targeted cell. **c**. Seahorse flux analysis of oxygen consumption rate (OCR) in cells after ND, ND + GGPP, and DPSC. Statistical significance, *** $p<0.001$, ** $p<0.01$, * $p < 0.05$ compared to DPSC controls. **d.**Seahorse flux analysis of extracellular acidification rate (ECAR) in cells after ND, ND + GGPP, and DPSC. Statistical significance, *** $p<0.001$, ** $p<0.01$, * $p < 0.05$ compared to DPSC controls.

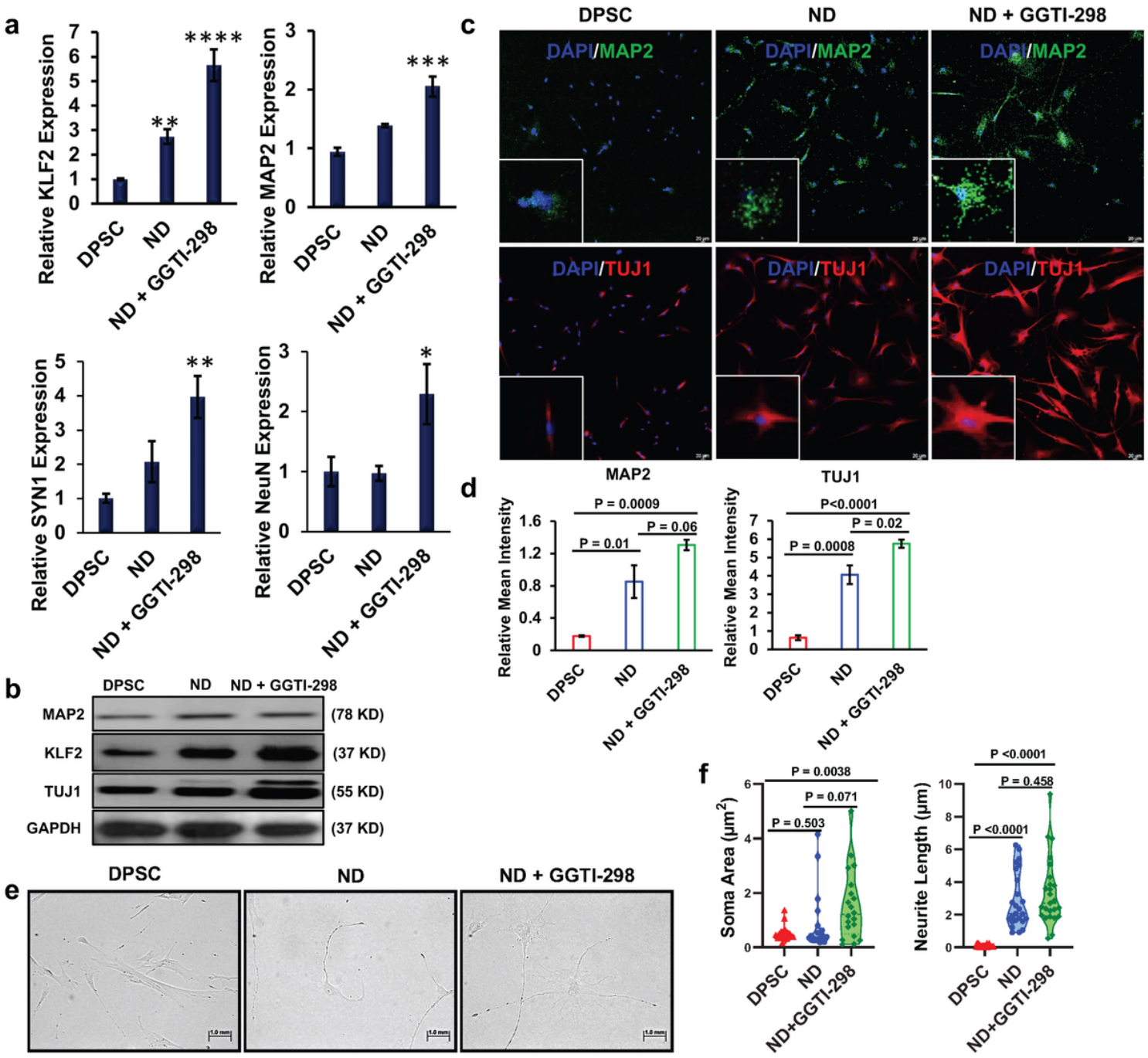

Figure 5

KLF2 overexpression induces neuronal differentiation. a. qRT-PCR analysis of KLF2, MAP2, SYN1, and NeuN was determined in cells after ND, ND + GGTI-298, and DPSC. Statistical significance, *** p<0.001, ** p<0.01, * p < 0.05 compared to DPSC controls. **b.** The protein level of KLF2, MAP2, TUJ1 and GAPDH as an internal control was determined by western blot. **c**. Immunofluorescence images of MAP2 (green) and TUJ1 (red) were shown. Inset represents a zoom view of targeted cell. **d**. Relative mean intensity of the images (n = 6). **e.** Bright-field images of cells after ND, ND + GGTI-298, and DPSC were shown. **f.** Graphs represent the quantitative evaluation of soma area (μm^2) and neurite length (μm) of the differentiated cells (n = 6).

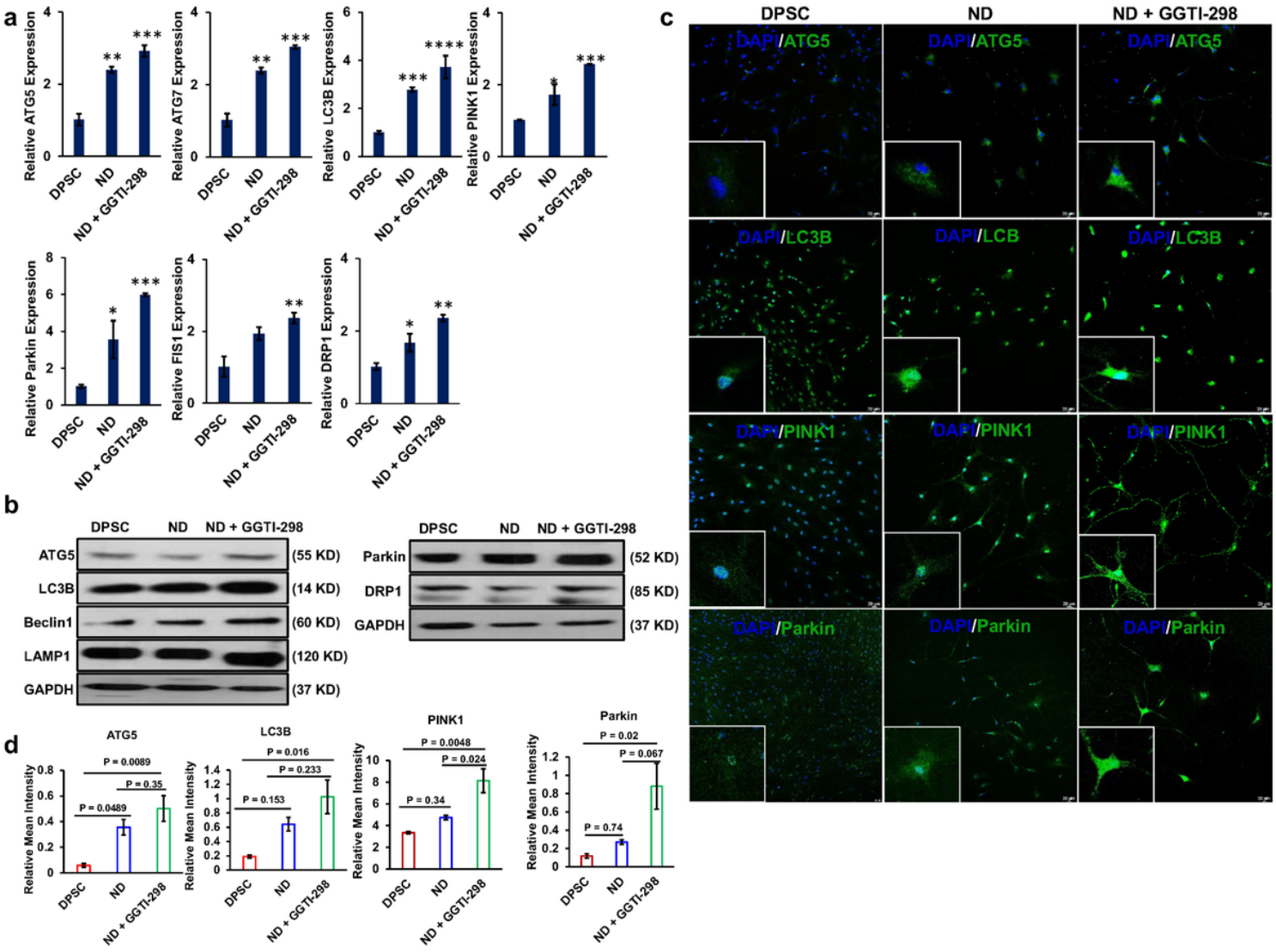

Figure 6

KLF2 overexpression induces autophagy, and mitophagy molecules. a. qRT-PCR analysis of ATG5, ATG7, LC3B, PINK1, Parkin, FIS1, DRP1 was determined in cells after ND, ND + GGTI-298, and DPSC. Statistical significance, *** p<0.001, ** p<0.01, * p < 0.05 compared to DPSC controls. **b.** The protein level of ATG5, LC3B, Beclin1, and LAMP1 (Left panel), Parkin1, and DRP1 (right panel) was determined by western blot, keeping GAPDH as an internal control. **c**. Immunofluorescence images of ATG5, LC3B, PINK1, and Parkin (green) were shown. Inset represents a zoom view of targeted cell. **d**. Relative mean intensity of the images (n = 6).

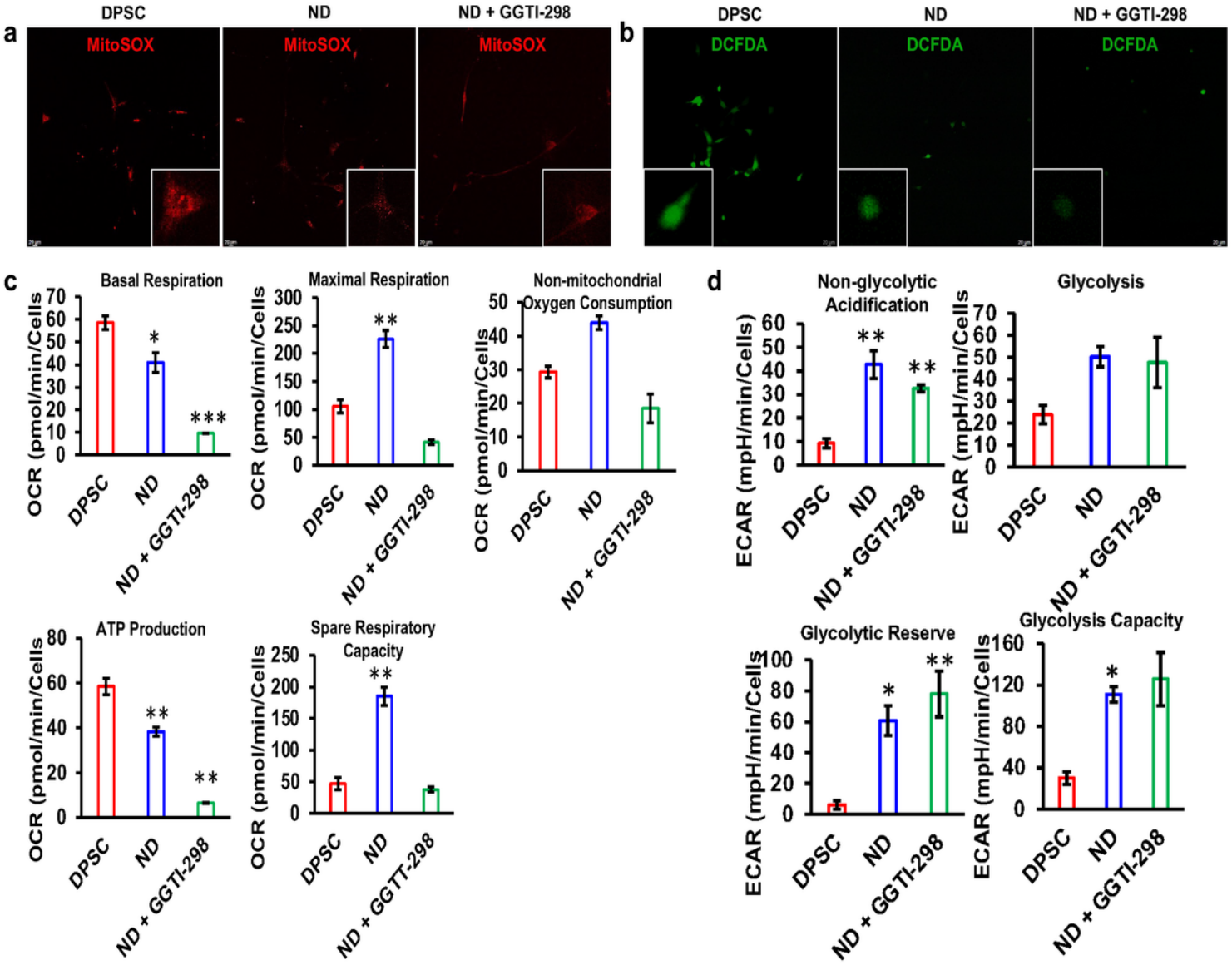

Figure 7

Effect of KLF2 sufficiency on redox signaling and cellular bioenergetics. a. MitoSOX-stained cells were shown after ND, ND + GGTI-298, and DPSC. Inset represents a zoom view of targeted cell. **b.** DCFDA-stained cells were shown after ND, ND + GGTI-298, and DPSC. Inset represents a zoom view of targeted cell. **c.**Seahorse flux analysis of oxygen consumption rate (OCR) in cells after ND, ND + GGTI-298, and DPSC. Statistical significance, *** $p<0.001$, ** $p<0.01$, * $p < 0.05$ compared to DPSC controls. **d.** Seahorse flux analysis of extracellular acidification rate (ECAR) in cells after ND, ND + GGTI-298, and DPSC. Statistical significance, *** $p<0.001$, ** $p<0.01$, * $p < 0.05$ compared to DPSC controls.

Supplementary Files

This is a list of supplementary files associated with this preprint. Click to download.

- nreditorialpolicychecklistflat.pdf

- PrateekshaetalSupplementaryFigures101322.docx
- SupplementaryFinalFigures92922.pdf
- GraphicalAbstract.tif